Asian Journal of Chemistry; Vol. 35, No. 9 (2023), 2171-2175

ASIAN JOURNAL OF CHEMISTRY

https://doi.org/10.14233/ajchem.2023.27794

Optical Properties of Heterostructured ZnO/NiO Nanocomposites Synthesized *via* Facile Precipitation Process

K. ANANDAN[1,*], K. RAJESH[1], K. GAYATHRI[1], ANITHA REXALIN DEVARAJ[1], M. MOHANBABU[2] and P. PRABHAKAR RAO[3]

[1]Department of Physics, Centre for Nanotechnology, Centre for Hydrogen Energy Research, AMET University, Kanathur, Chennai-603112, India
[2]Department of Physics, Sri Malolan College of Arts and Science, Madhurantakam, Kanchipuram-603306, India
[3]Materials Science and Technology Division, National Institute for Interdisciplinary Science and Technology (NIIST), Thiruvananthapuram-695019, Inida

*Corresponding author: E-mail: anand.nanoscience@yahoo.com; anand.ka@ametuniv.ac.in

Received: 14 March 2023; *Accepted*: 14 July 2023; *Published online*: 31 August 2023; AJC-21360

The semiconductor zinc oxide/nickel oxide (ZnO/NiO) heterostructured nanocomposites have been successfully synthesized *via* facile and eco-friendly homogeneous precipitation process with ethanol and water as solvents. The prepared nanocomposites were studied by means of structural and optical characteristics by using X-ray diffraction, ultraviolet visible absorption and photoluminescence emission spectro-scopies. The peaks in the XRD pattern attributed to the hexagonal wurtzite structure of ZnO and face-centered cubic structure of NiO, as a result the XRD analysis further confirmed that the solvents play a powerful role in size of the crystallite of the synthesized nanocomposites. Strong UV absorption may be seen in UV-vis absorbance spectra and samples of ZnO/NiO nanocomposite materials had greater energy gap (E_g) values than those of pure NiO and ZnO materials. The synthesized materials have demonstrated high photoluminescence emission in UV-blue region in the range of 241-498 nm, it might be a valuable source for future display applications. According to the aforementioned finding, the ZnO/NiO nanocomposites showed significant promise and were a viable material for optoelectronic devices.

Keywords: Semiconductors, Metal oxides, Nanocomposites, Precipitation process, Optical properties.

INTRODUCTION

Nanoparticles have received a lot of interest because of their multifunctionality, including optical, electrical, magnetic and catalytic properties, *etc*. Electronic characteristics of nanocrystalline materials are significantly influenced by their structure [1]. Due to their high surface to volume ratio, they require substantial preparation. In recent years, both basic research and technical applications have focused mainly on semiconductor nanocrystals [1-3]. Metal oxide nanoparticles' structure and features, particularly those related to their size and shape, have a significant impact on how well they perform functionally in the applications for which they are used. Additionally, because to the quantum confinement effect, they possess special size-dependent optical and electrical features [4,5].

The p- and n-type semiconductors combine to generate mixed metal oxide nanostructures, which are particularly significant due to their distinct physical and chemical characteristics that set them apart from the separate metal oxides. Among the nanostructured semiconductors, zinc oxide is a versatile, well-known, non-toxic, low cost semiconductor metal oxide as it has novel optical, electrical, catalytic and photocatalytic features as well as a large direct band gap (3.37 eV), a high exciton binding energy of 60 meV at ambient temperature and other very desirable physical characteristics [6,7]. Among the various nanocomposites materials, ZnO/NiO coupled systems have been receiving lot of attention, because of the matching electronic band positions of ZnO and NiO. Nickel oxide (NiO) is a p-type semiconducting oxide with a 3.5 eV band gap, excellent hole mobility and minimal lattice misfit with ZnO [8]. As a result, NiO is an appropriate option for coupling with ZnO to generate p-n heterostructures. The development of heterojunctions between n-type ZnO and an appropriate p-type semiconducting oxide can improve the optical characteristics of

nanocomposites [9]. Nanocomposites of semiconducting oxides are recognized to have highly fascinating chemical and physical characteristics and are used in a variety of applications in the field of optoelectronics [10].

In present work, an easily route and cost-effective process for the preparation of ZnO/NiO heterostructured nanocomposites. The optical characteristics of ZnO/NiO nanocomposites have been systematically investigated. The results show that n-type ZnO/p-type NiO hetrojunctions have better optical characteristics than ZnO, NiO and their physical combination.

EXPERIMENTAL

All of the chemicals were commercial, had high AR purity and were utilized without additional purification. The ZnO/NiO composites were synthesized using a simple precipitation method. In a standard synthesis, 1:2 ratio of metal acetate and sodium hydroxide were used. For ethanol mediated ZnO/NiO nanocomposite synthesis, four 25 mL of ethanol were taken in four different beakers. Solution 1: in first two beakers, 0.1 M (0.5485 g) of zinc acetate dihydrate ($Zn(CH_3COO)_2{\cdot}2H_2O$) and 0.2 M of (0.1999 g) NaOH pellets were dissolved under stirring separately. The $Zn(OH)_2$ precipitates were obtained, when these two 25 mL of solutions were slowly added together under stirring. Similarly, solution 2: in the second two beakers 0.1 M (0.6221 g) of nickel acetate tetrahydrate ($Ni(CH_3COO)_2{\cdot}4H_2O$) and 0.2 M of (0.1999 g) NaOH pellets were dissolved under stirring separately. The $Ni(OH)_2$ precipitates were obtained, when these two 25 mL of solutions were slowly added together under stirring. After the 10 min of stirring, the precipitated solutions 1 and 2 were mixed under vigorous stirring, for which stirring was done for 1 h. The resulting precipitate was filtered, cleaned of contaminants using distilled water and 100% ethanol, then dried for 12 h at 120 ºC. The ZnO/NiO sample was then produced in light greenish coloured after being calcined at 450 ºC for 2 h. The water-mediated ZnO/NiO sample was also prepared using the exact same method. The following equation describes the general production of ZnO/NiO nanocomposites:

$$\left.\begin{matrix} Zn(CH_3COO)_2{\cdot}2H_2O \\ + \\ Ni(CH_3COO)_2{\cdot}4H_2O \end{matrix}\right\} + 4NaOH \longrightarrow \begin{matrix} Zn(OH)_2/Ni(OH)_2 \\ + \\ 4(NaCH_3COO) + 6H_2O \end{matrix}$$

$$Zn(OH)_2/Ni(OH)_2 \longrightarrow ZnO/NiO + 2H_2O$$

Characterization: To obtain about the structural as well as optical properties of synthesized ZnO/NiO nanocomposites to do structural and optical characterizations such as X-ray diffractions (XRD), ultraviolet-visible (UV-Vis) and photoluminescence (PL) spectroscopes. XRD analysis, which measures based on the dual characteristic *i.e.* crystallite as well as the wavenature of X-rays, is used to get the structural information regarding the crystallite structure, nature and size of the synthesized metal oxide nanocomposites. The X-ray diffractometer (XPERT-PRO) was used to analyze the structural properties of nanocomposites for 2θ values ranging from 20º to 80º at 40 Kv and 30 mA operating with Cu*K*α as the radiation source (λ = 0.154178 nm) with a scanning speed of 2º/min at room temperature. By analyzing 2θ patterns and using the Scherrer formula, crystallite size in nm was determined from fullwidth at half maximum (FWHM). The optical features of the synthesized ZnO/NiO nanocomposites were performed by using a ultraviolet visible (UV-Vis) and photoluminescence (PL) spectroscopies. The ultraviolet-visible (Varian Cary 5E spectrophotometer) absorption spectra of ZnO/NiO were captured between 200 and 800 nm. Using a Fluoromax-4 spectrofluorometer and a room-temperature Xenon lamp as an excitation light source, the photoluminescence spectra of emission were measured between 200 and 600 nm.

RESULTS AND DISCUSSION

XRD studies: The powder XRD patterns of the synthesized nanocomposite (ZnO/NiO) by using two different solvents are shown in Fig. 1, which reveals that the combination of ZnO and NiO diffraction peaks. Hence, it is concluded that the synthesized materials are nanocomposite not a single metal oxide nanomaterials. The sharpened peaks of the XRD patterns indicating that the highly crystalline quality of the synthesized nanocomposite materials. The peaks appeared at 2θ values of 31.78º, 34.44º, 36.27º, 47.58º, 56.62º, 66.39º, 67.99º, 69.14º, 72.96º and 77.02º belong to the planes of (100), (002), (101), (102), (110), (200), (112), (201), (004) and (202), which are associated with the hexagonal phase of ZnO structure, similarly, the peaks at 37.05º, 43.04º, 62.52º, 74.94º and 78.9º correspond to (111), (200), (220), (311) and (222) planes of face centered cubic of the NiO crystal, respectively. Moreover, which are well agreed with standard ZnO JCPDS No. 76-0704 and NiO JCPDS No. 00-047-1049 [11]. No diffraction peaks were observed for impurity, it further shown that the heterostructure's ZnO and NiO composition. The wider width of the diffraction peaks of the ethanol mediated sample (Fig. 1a) indicates that the synthesized ZnO/NiO nanocomposite has a smaller size in crystallites. For convenience of observation of the wider width of the diffraction peaks, one single peak (2θ = 43.04º) is enlarged for both samples which are depicts in Fig. 2. The results indicated that there was a noticeable decrease in diffraction peak intensity

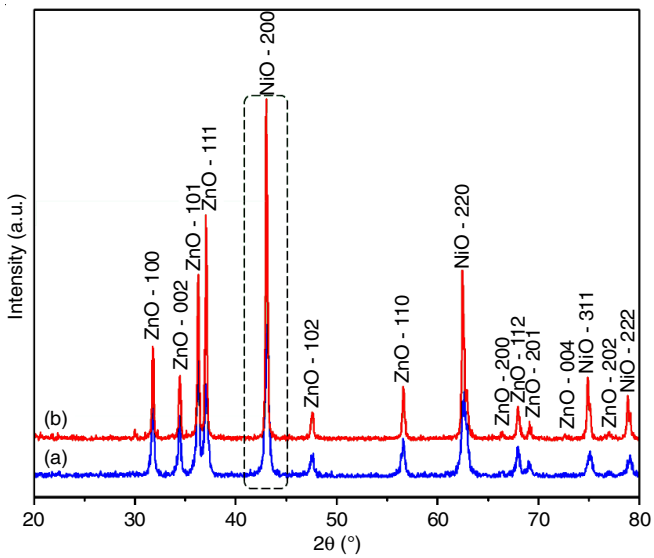

Fig. 1. XRD patterns of (a) ethanol and (b) water mediated ZnO/NiO nanocomposites

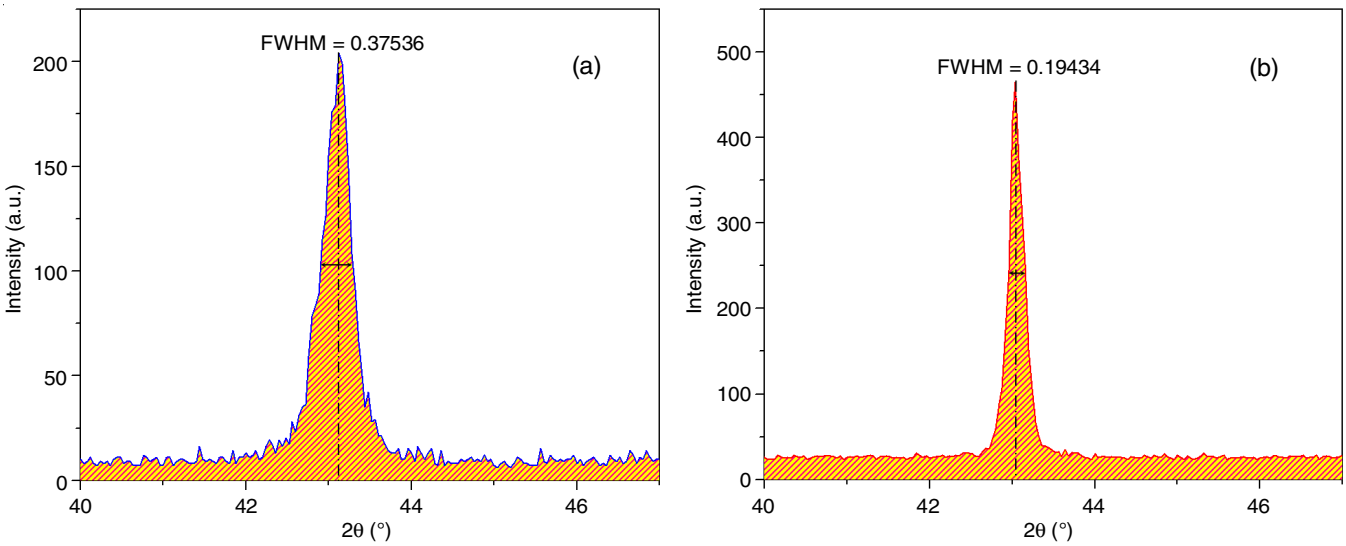

Fig. 2. FWHM for (a) ethanol and (b) water mediated ZnO/NiO nanocomposites

as the full width at half maximum (FWHM) value increased for the ethanol-mediated sample (FWHM = 0.37536) compared to the water-mediated sample (FWHM = 0.19434). This decrease in intensity can be attributed to a reduction in the crystallite size of the sample.

The broadening effects of the instrument and sample are the main reasons of broadness of diffraction peaks in the XRD pattern. In order to separate the line widening caused by the instrument from that of the sample, a reference material like silicon must be recorded. The adjusted and corrected broadening (b) of the diffraction peaks in the samples was determined using the following formula [12]:

$$\beta = [\beta^2_{measured} - \beta^2_{instrumental}]^{1/2}$$

The mean crystallite sizes of the synthesized ZnO/NiO nanocomposite were measured by using Scherrer's formula:

$$D = \frac{K\lambda}{\beta \cos\theta}$$

where D is the mean crystallite size of sample, λ = 0.154178 nm is the wavelength of Cu*K*α, β is the intensity of full width at half maximum (FWHM) of the peak, Bragg's diffraction angle is θ and constant K is set as 0.94. The average crystallite diameters of both the water and ethanol assisted ZnO/NiO nanocomposites are found to be 25.10 and 38.67 nm, respectively.

The final product qualities were mainly influenced by reaction conditions such as solvent, temperature and processing time. For example, particle size might be adjusted by utilizing different solvents with varying boiling points. The influence of the solvent's boiling point on the size of nanoparticles will be a crucial factor [13]. It is interesting to observe that when the boiling point of the employed solvent dropped, the average size of the particles of ZnO/NiO nanocomposites also reduced. Due to the lower boiling point of ethanol (78.4 ºC) mediated samples show lower crystallite sizes than that of water (100 ºC) mediated samples. Since the solvents evaporated at a faster pace due to their lower boiling temperatures, they helped the prepared solution generate a large number of nuclei. Additionally, a huge number of nuclei are transformed into tiny nanoparticles [14,15]. As a result of their superior dispersion and capping abilities, the ethanol assisted ZnO/NiO nanocomposites are the most ultra-fine. Moreover, Uekawa *et al.* [16] proposed that in the process of synthesizing nanomaterials, the crystallite growth is inhibited in pure ethanol solution.

UV-visible studies: Fig. 3 depicts the UV-visible absorption spectra of different kind of solvent-mediated ZnO/NiO nanocomposites. The optical absorption below 400 nm exhibited by both ZnO and NiO signifies their capacity for ultraviolet (UV) absorption. The UV-vis absorption spectra of the synthesized nanocomposites shows strong peak at 352 nm in the UV region, which are due to the electron transitions from the valence band to the conduction band as well defects levels of the materials [17]. The UV absorption ability of the materials is exhibited by the strong absorption in the UV region. Moreover, the absorption intensity higher for the ethanol mediated ZnO/NiO nanocomposites than that of water mediated sample, which might be associated with the smaller crystallite sizes of the sample. The metal oxide nanocomposites more effectively absorb the UV light than that of pure metal oxide nanoparticles [18]. The following equation was used to compute the optical band gap energy [19]:

$$(\alpha h\nu) = A\,(h\nu - E_g)^n$$

where A is a proportionality constant, E_g is a material's band gap; ν is the frequency of incoming radiation; h is Planck's constant and n represents the type of the sample transitions [20]. The plot of $(\alpha h\nu)^2$ *vs.* photon energy (hν) of ZnO/NiO nanocomposites is shown in Fig. 4. The optical band gaps of ZnO/NiO nanocomposites were found to be 3.54 and 3.62 eV for water and ethanol mediated samples, respectively. The determined band gaps of the ZnO/NiO nanocomposites are greater than those of the bulk materials and are in good agreement with the reported values [21]. The observed blue shift in the optical band gap energy of the ZnO/NiO nanocomposite, as compared to the bulk forms of ZnO and NiO, can be attributed to the band-bending effect induced by the smaller size of the

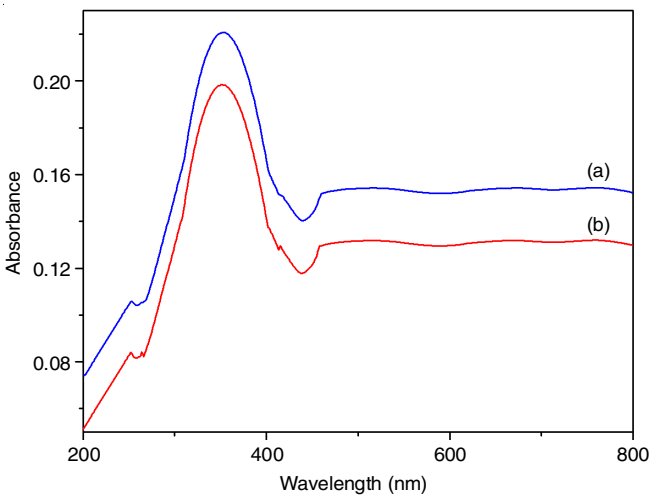

Fig. 3. UV-vis absorption spectra of (a) ethanol and (b) water mediated ZnO/NiO nanocomposites

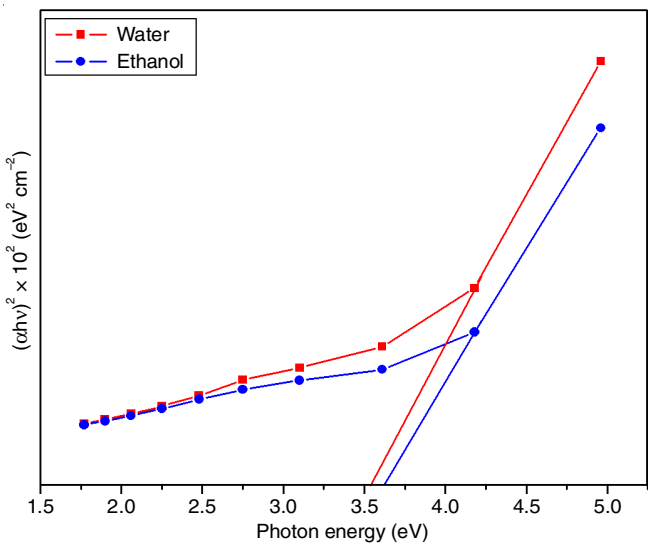

Fig. 4. $(\alpha h\nu)^2$ *versus* photon energy (hν) plot of ZnO/NiO nanocomposites

crystallites. The greater the surface-to-volume ratio of particles at the nanoscale, the greater the impact of band bending [22]. Moreover, increasing band gap energy values with smaller crystallite size of the ethanol mediated sample indicating that the quantum confinement effect of the synthesized ZnO/NiO nanocomposites [23].

Photoluminescence studies: In order to examine the inherent crystal defects present in the semiconductor metal oxide nanocomposite samples, such as Ni and Zn vacancies, interstitial metal and oxygen vacancies, the photoluminescence (PL) emission technique was employed. It was found that the emission bands were present in the UV-blue range (Fig. 5). A broad and strong UV-blue emission is observed in the range of 241-498 nm, the greatest emission intensity verified that the materials were good crystallinity and further, defects level of the samples and crystallite size of the samples plays a vital role in the peak intensity of the photoluminescence spectra. From the PL spectra, the ethanol mediated ZnO/NiO nanocomposites shows broad and high intense spectrum than that of water mediated sample, which due to smaller crystallite size

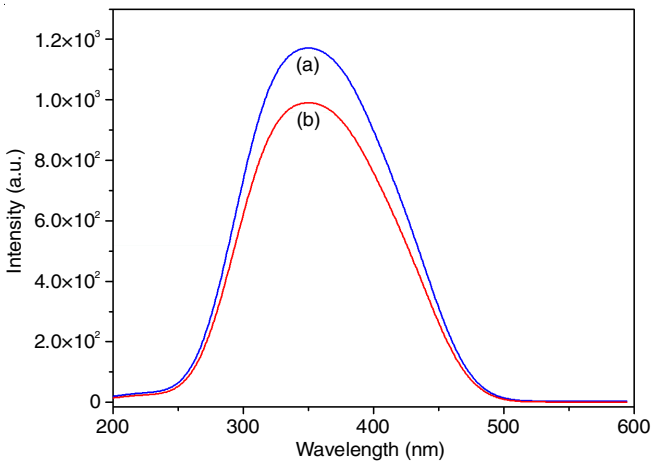

Fig. 5. Photoluminescence emission spectra of (a) ethanol and (b) water mediated ZnO/NiO nanocomposites

of the sample. Many hypotheses have been put forth regarding the origin of the broad UV-blue emission, including the transfer of electrons from oxygen vacancies (VO) to the valence band (VB), metal interstitials (Mi) to metal vacancies (VM) and Mi to the VB or -OH groups at the particle surface and these varies depending on the synthesis method used [24-27]. In addition, the near-band edge UV-blue emission, which occurs in the 241-498 nm range, is caused by the radiative recombination of an excited electron in the conduction band with the valence band hole or the band-band PL spectrum. The presence of oxygen-depleted, deep-level interface traps may be responsible for the peak associated with UV-blue emission, which led to the creation of new electronic energy levels between the bands of conduction and valence [28]. Because all of these flaws are acceptors in nature and acceptor-to-acceptor transfer is prohibited, the only viable channel for UV-blue emission is that from the CB to an acceptor. So, the enhancement of the UV-blue luminescence of the synthesized metal oxide nanocomposite is attributed to the elimination of the competing routes to the UV light emission due to defects [29].

Conclusion

In conclusion, this work illustrates the effective and successful synthesis of ZnO/NiO heterostructured nanocomposite *via* eco-friendly precipitation process with ethanol and water as solvents and structural and optical properties of the products were fully analyzed. The X-ray diffraction pattern of ZnO/NiO coupled metal oxide nanocomposites exhibited two set of strong and sharp diffraction peaks, which correspond to hexagonal wurtzite and FCC structured ZnO and NiO. The crystallite size of the samples were calculated, ethanol mediated samples shows smaller in size than that of water mediated sample. The optical band gap of ZnO/NiO nanocomposites (E_g = 3.54 and 3.62 eV for water and ethanol mediated samples), which are higher than that of bulk ZnO and NiO. The synthesized nanocomposites exhibit a prominent UV-blue emission peak in the range of 241-498 nm may be attributed to their high crystallinity and the absence of alternative pathways for UV light emission. This can be related to the smaller size of the crystallites and the reduced presence of defects within the

samples. Thus, the synthesized metal oxide nanocomposites confirmed that the solvents used to synthesize the nanomaterials play an important role. Hence, eco-friendly precipitation process is a facile and appropriate method towards preparation of semiconductor metal oxide nanocomposites with tunable structural and optical properties in view of their potential in optoelectronics devices applications.

CONFLICT OF INTEREST

The authors declare that there is no conflict of interests regarding the publication of this article.

REFERENCES

1. J. Fang, Z. Zhou, M. Xiao, Z. Lou, Z. Wei and G. Shen, *InfoMat*, **2**, 291 (2020); https://doi.org/10.1002/inf2.12067
2. W.A.A. Mohamed, H. Abd El-Gawad, S. Mekkey, H. Galal, H. Handal, H. Mousa and A. Labib, *Nanotechnol. Rev.*, **10**, 1926 (2021); https://doi.org/10.1515/ntrev-2021-0118
3. D. Jasrasaria, D. Weinberg, J.P. Philbin and E. Rabani, *J. Chem. Phys.*, **157**, 020901 (2022); https://doi.org/10.1063/5.0095897
4. A.P. Alivisatos, *Science*, **271**, 933 (1996); https://doi.org/10.1126/science.271.5251.933
5. H. Weller, *Adv. Mater.*, **5**, 88 (1993); https://doi.org/10.1002/adma.19930050204
6. X. Xu, F. Xia, L. Zhang and J. Gao, *Sci. Adv. Mater.*, **7**, 423 (2015); https://doi.org/10.1166/sam.2015.2132
7. I. Ibrahim, H.N. Lim, S.S. Sharifuddin, M.A.M. Yusof, N.M. Huang and A. Pandikumar, *Sci. Adv. Mater.*, **7**, 1556 (2015); https://doi.org/10.1166/sam.2015.2288
8. Y. Liu, G. Li, R. Mi, C. Deng and P. Gao, *Sens. Actuators B Chem.*, **191**, 537 (2014); https://doi.org/10.1016/j.snb.2013.10.068
9. S. Nandi, S. Kumar and A. Misra, *Mater. Adv.*, **2**, 6768 (2021); https://doi.org/10.1039/D1MA00670C
10. X. Yu, T. Marks and A. Facchetti, *Nature Mater.*, **15**, 383 (2016); https://doi.org/10.1038/nmat4599
11. H. D. Weldekirstos, B. Habtewold and D. M. Kabtamu, *Front. Mater.*, **9**, 832439 (2022); https://doi.org/10.3389/fmats.2022.832439
12. T. Tangcharoen, W. Klysubun and C. Kongmark, *J. Mol. Struct.*, **1156**, 524 (2018); https://doi.org/10.1016/j.molstruc.2017.12.019
13. K. Anandan, K. Rajesh and V. Rajendran, *J. Mater. Sci. Mater. Electron.*, **28**, 17321 (2017); https://doi.org/10.1007/s10854-017-7664-1
14. R. Kumar, P.F. Siril and P. Soni, *Propellants Explos. Pyrotech.*, **39**, 383 (2014); https://doi.org/10.1002/prep.201300104
15. T. Hyeon, *Chem. Commun.*, **8**, 927 (2003); https://doi.org/10.1039/b207789b
16. N. Uekawa, M. Kitamura, S. Ishii, T. Kojima and K. Kakegawa, *J. Ceram. Soc. Jpn.*, **113**, 439 (2005); https://doi.org/10.2109/jcersj.113.439
17. Q. Zhu, C. Xie, H. Li, C. Yang, S. Zhang and D. Zeng, *J. Mater. Chem. C*, **2**, 4566 (2014); https://doi.org/10.1039/C4TC00011K
18. E. Lizundia, I. Armentano, F. Luzi, F. Bertoglio, E. Restivo, L. Visai, L. Torre and D. Puglia, *ACS Appl. Bio Mater.*, **3**, 5263 (2020); https://doi.org/10.1021/acsabm.0c00637
19. K. Samudrala and S.B. Devarasetty, *Conf. Ser.: Mater. Sci. Eng.*, **330**, 012042 (2018); https://doi.org/10.1088/1757-899X/330/1/012042
20. M.A. Butler, *J. Appl. Phys.*, **48**, 1914 (1977); https://doi.org/10.1063/1.323948
21. A.I. Hassan and A.M. Yahya, *AIP Confer. Proceed.*, **2213**, 020208 (2020); https://doi.org/10.1063/5.0000253
22. A. Albanese, P.S. Tang and W.C.W. Chan, *Annu. Rev. Biomed. Eng.*, **14**, 1 (2012); https://doi.org/10.1146/annurev-bioeng-071811-150124
23. P. Singh, R.K. Singh and R. Kumar, *RSC Adv.*, **11**, 2512 (2021); https://doi.org/10.1039/D0RA08670C
24. L. Zhang, L. Yin, C. Wang, N. Lun, Y. Qi and D. Xiang, *J. Phys. Chem. C*, **114**, 9651 (2010); https://doi.org/10.1021/jp101324a
25. C.H. Ahn, Y.Y. Kim, D.C. Kim, S.K. Mohanta and H.K. Cho, *J. Appl. Phys.*, **105**, 013502 (2009); https://doi.org/10.1063/1.3054175
26. M. Abdullah, I.W. Lenggoro, K. Okuyama and F.G. Shi, *J. Phys. Chem. B*, **107**, 1957 (2003); https://doi.org/10.1021/jp022223c
27. S. Monticone, R. Tufeu and A.V. Kanaev, *J. Phys. Chem. B*, **102**, 2854 (1998); https://doi.org/10.1021/jp973425p
28. S. Baskoutas and G. Bester, *J. Phys. Chem. C*, **115**, 15862 (2011); https://doi.org/10.1021/jp204299m
29. K. Anandan, K. Rajesh, K. Gayathri, S. Vinoth Sharma, S.G.M. Hussain and V. Rajendran, *Physica E*, **124**, 114342 (2020); https://doi.org/10.1016/j.physe.2020.114342